J Solid State Electrochem (2008) 12:105–111
DOI 10.1007/s10008-007-0367-4

ORIGINAL PAPER

Effect of different conductive additives on charge/discharge properties of $LiCoPO_4$/Li batteries

Bo Jin · Hal-Bon Gu · Ki-Won Kim

Received: 16 March 2007 / Revised: 13 April 2007 / Accepted: 29 May 2007 / Published online: 4 July 2007

Abstract Single-phase $LiCoPO_4$ nanoparticles were synthesized by solid-state reaction method and subsequent high-energy ball milling. The electrochemical properties of $LiCoPO_4$/Li batteries were analyzed by ac impedance experiments, cyclic voltammetry (CV), and charge/discharge tests. The structural and morphological performance of $LiCoPO_4$ nanoparticles was investigated by X-ray diffraction (XRD), scanning electron microscope (SEM), and transmission electron microscope (TEM). The XRD result demonstrated that $LiCoPO_4$ nanoparticles had an orthorhombic olivine-type structure with a space group of Pmnb. Different conductive additives including acetylene black and carbon black (SP270) were used to fabricate electrodes. The morphologies of the electrodes and different conductive additives were observed by field emission-scanning electron microscopy (FE-SEM). $LiCoPO_4$/Li battery with acetylene black showed the best electrochemical properties, and exhibited a discharge plateau at around 4.7 V with an initial discharge capacity of 110 mAh g^{-1} at a discharge current density of 0.05 mA cm^{-2} at 25 °C.

Keywords Olivine · Lithium-ion batteries · Solid-state reaction · Conductive additives · High-energy ball milling

B. Jin (✉) · H.-B. Gu
Department of Electrical Engineering,
Chonnam National University,
300 Yongbong-dong, Buk-gu,
Gwangju 500-757, South Korea
e-mail: jinbo@jlu.edu.cn

K.-W. Kim
ITRC for Energy Storage and Conversion,
Gyeongsang National University,
Jinju 660-701, South Korea

Introduction

Since the commercialization of rechargeable lithium-ion batteries by Sony Energy Tech. [1] 16 years ago, they have been widely utilized as the power sources in a wide range of applications, such as mobile phones, laptop computers, and cameras. In the rechargeable lithium-ion batteries, cathode material is the key component, and mainly devoted to the performance of the batteries. Among the known cathode materials, the layered $LiCoO_2$, $LiMnO_2$, and $LiNiO_2$, spinel $LiMn_2O_4$, and other cathode materials such as elemental sulfur have been studied extensively [2–10]. $LiCoO_2$ has been nowadays utilized for commercial lithium-ion batteries. However, novel cathode material must be developed not only in relation to battery performance, but also in relation to safety and cost.

Recently, lithium transition metal phosphates with an ordered olivine-type structure, $LiMPO_4$ (M = Fe, Mn, Ni, and Co), have attracted extensive attention because of high theoretical specific capacity (≈170 mAh g^{-1}) [11–19]. The potential of the M^{3+}/M^{2+} redox couple vs Li/Li^+ of $LiMPO_4$ is as follows; 3.5 V for $LiFePO_4$, 4.1 V for $LiMnPO_4$, 5.2–5.4 V for $LiNiPO_4$, and 4.8 V discharge plateau for $LiCoPO_4$. In $LiCoPO_4$, the oxidation state of Co^{4+} does not form in the reversible oxidation/reduction reaction. $LiCoPO_4$ is a very promising candidate as a cathode material for lithium-ion batteries because of its high voltage (4.8 V vs Li/Li^+). Although its theoretical capacity is 167 mAh g^{-1}, the reported values are low (70 [13] and 100 mAh g^{-1} [14]).

The high-energy ball-milling process is a promising method for synthesizing cathode materials [20–22]. During the high-energy ball-milling process, the powder particles undergo repeated welding, fracturing, and rewelding in a dry high-energy ball-milling vessel. This results in pulverization, intimate powder mixing [20]. An improvement in electronic

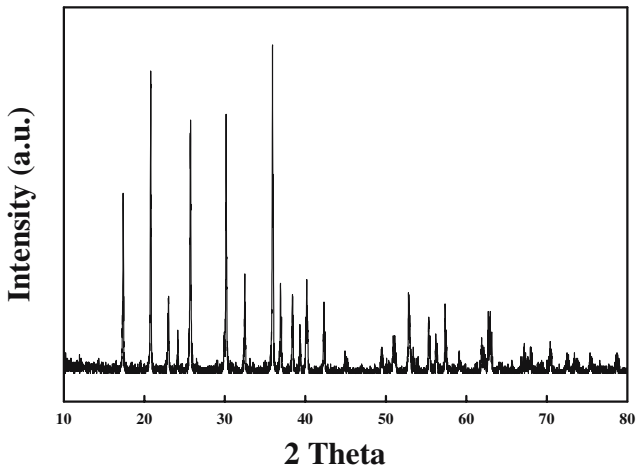

Fig. 1 XRD pattern for $LiCoPO_4$ nanoparticles

conductivity of $LiCoPO_4$ prepared by the high-energy ball-milling process can be expected due to the very fine nanoparticles and their large specific surface area.

In this study, therefore, single phase $LiCoPO_4$ nanoparticles were synthesized by solid-state reaction method and subsequent high-energy ball-milling process. Different conductive additives including acetylene black and carbon black (SP270) were added during making electrodes. The electrochemical properties of $LiCoPO_4$ nanoparticles were analyzed by means of SEM, FE-SEM, TEM, XRD, CV, ac impedance experiments, and charge/discharge tests.

Experimental

$LiCoPO_4$ nanoparticles were synthesized from a stoichiometric mixture of $LiOH{\cdot}H_2O$, CoO, and $(NH_4)_2HPO_4$ using a solid-state reaction method and subsequent high-energy ball-milling process. First, the mixture was ground in an agate mortar and pressed into a pellet at a pressure of 650 kgf cm^{-2}, and then fired in air at 750 °C for 8 h. After cooling, the resulting material was again calcined slowly at 350 °C for 6 h. Finally, the material was cooled and ground into powder, and a pellet was again made by pressing at a pressure of 650 kgf cm^{-2} before being heated at 750 °C for 36 h. After cooling, the resulting material was again ground into powder. The resulting $LiCoPO_4$ nanoparticles were prepared by the high-energy ball-milling process for 10 h using a shaker type of ball mill (Planetary Mono Mill) that rotated at 300 rpm. The ball-to-powder weight ratio was 20:1.

The cathodes were made from mixtures of $LiCoPO_4$, acetylene black or carbon black (SP270), and polyvinylidene fluoride binder dissolved in *N*-methylpyrrolidinone in a weight ratio of 70:25:5. The slurry was ball-milled for 1 h, and then coated onto an Al foil. The resulting electrode film was pressed with a twin roller, cut into a rectangle plate (area=4 cm^2), and dried at 110 °C for 24 h under vacuum. Lithium cells were constructed with a separator made from Celgard2500 membrane, the cathode with an area of 4 cm^2, and anode of lithium metal. The test cells were cycled galvanostatically in a potential range of 3.0–5.1 V using a

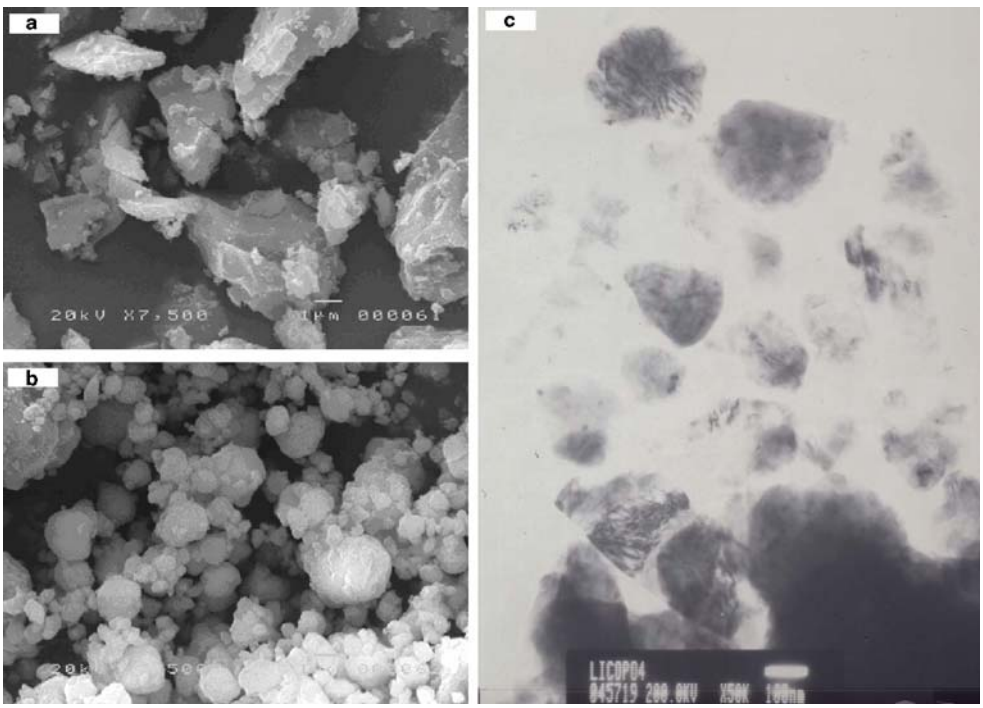

Fig. 2 SEM images of $LiCoPO_4$ nanoprticles (**a**) before the high-energy ball-milling process, (**b**) after the high-energy ball-milling process, and (**c**) TEM image of **b**

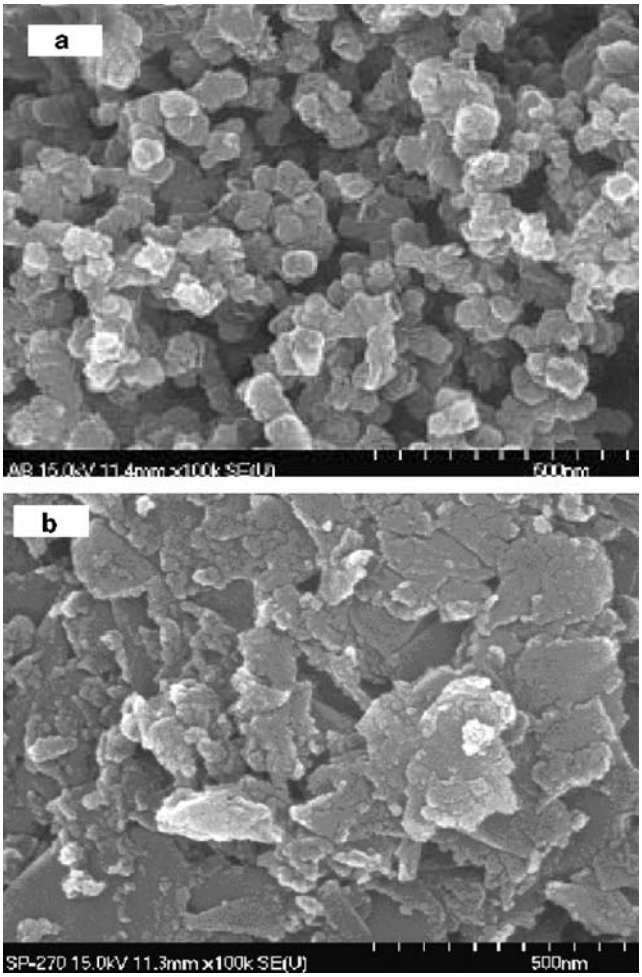

Fig. 3 FE-SEM images of different conductive additives (**a**) acetylene black and (**b**) carbon black (SP270)

WBCS3000 (Wonatech) Battery Tester System at different current densities ranging from 0.05 to 0.80 mA cm^{-2} at 25 °C. The electrolyte solution was 1 M $LiPF_6$ dissolved in a 50:50 vol.% mixture of ethylene carbonate (EC) and diethyl carbonate (DEC).

The crystalline phases were identified with X-ray diffraction (XRD, Dmax/1200, Rigaku) using Cu Kα radiation. The WBCS3000 (Wonatech) Battery Tester System was also used for measurements of cyclic voltammetry at a scan rate of 0.1 mV s^{-1}. The morphology of $LiCoPO_4$ nanoparticles was examined with a JEOL JSM-5400 SEM which had an accelerating voltage of 20 kV and a JEOL JEM-2000 TEM which had an accelerating voltage of 200 kV. The morphology of electrode was observed with a Hitachi S-4700 FE-SEM which had an accelerating voltage of 15 kV. Electrochemical impedance spectrum (EIS) measurements were performed using an IM6 impedance system (Zahner Elektrik Company). The spectrum was potentiostatically measured by applying an ac voltage of 20 mV over the frequency range from 2 to 10 MHz. $LiCoPO_4$ was used as working electrode and the lithium as both the counter and reference electrode.

Results and discussion

XRD pattern for $LiCoPO_4$ nanoparticles is shown in Fig. 1. The pattern can be indexed to a single-phase material having an orthorhombic olivine-type structure (space group Pmnb) with unit cell parameters: a=5.922, b=10.206, c=4.701 Å, and V=284.13 $Å^3$, which is the same as those listed in the JCPDS card. No impurity is found in the $LiCoPO_4$ nanoparticles. This structure may be described as chains (along the c direction) of edge-sharing cobalt-centered octahedra connected to one another by phosphate tetrahedra. These $(CoPO_4)^-$ are connected to one another by octahedrally coordinated lithium atoms along the b axis [13]. The diffraction peaks are prominent and its enhanced degree of crystallinity and better phase purity have been

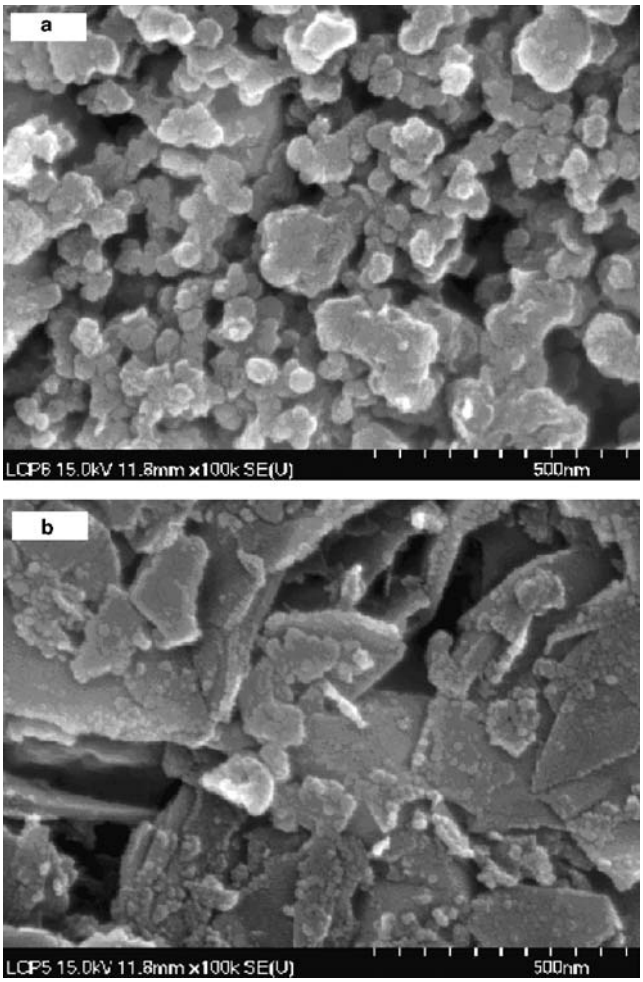

Fig. 4 FE-SEM images of the electrodes with different conductive additives (**a**) acetylene black and (**b**) carbon black (SP270)

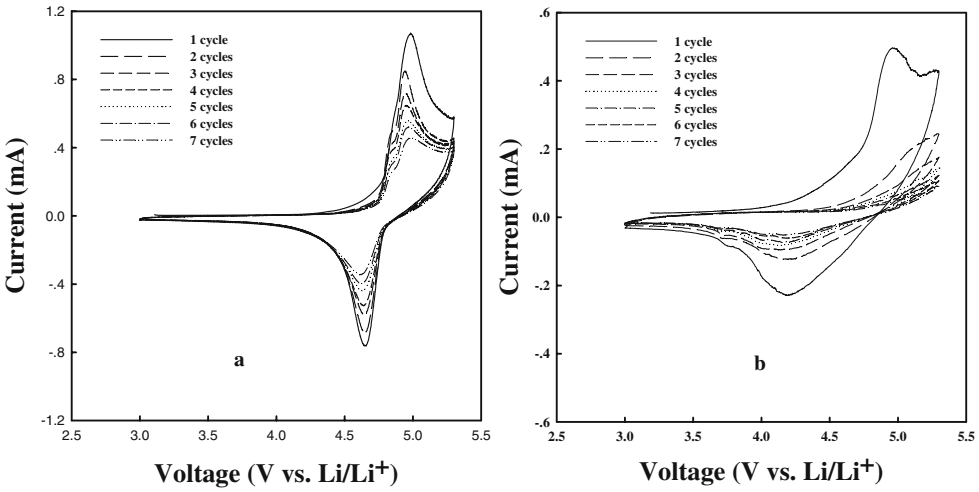

Fig. 5 Cyclic voltammograms of $LiCoPO_4$/Li batteries with different conductive additives (**a**) acetylene black and (**b**) carbon black (SP270)

demonstrated, which are evident from the sharp and symmetric diffractograms of increased intensity.

SEM and TEM images of $LiCoPO_4$ nanoparticles are shown in Fig. 2. As shown in Fig. 2a, the grain size of $LiCoPO_4$ powders ranges from 0.5 to 5 μm before the high-energy ball-milling process, and decreases to around 90–100 nm after the high-energy ball-milling process as shown in Fig. 2b and c. The $LiCoPO_4$ nanoparticles after the high-energy ball-milling process are spherical and more finely dispersed. It has been demonstrated that the high-energy ball-milling process provides an effective method in terms of homogeneity and particle size. In particles with a small diameter, lithium ions diffuse over smaller distances between the surfaces and center during lithium intercalation and deintercalation, and the $LiCoPO_4$ on the particle surfaces contributes mostly to the charge/discharge reac-

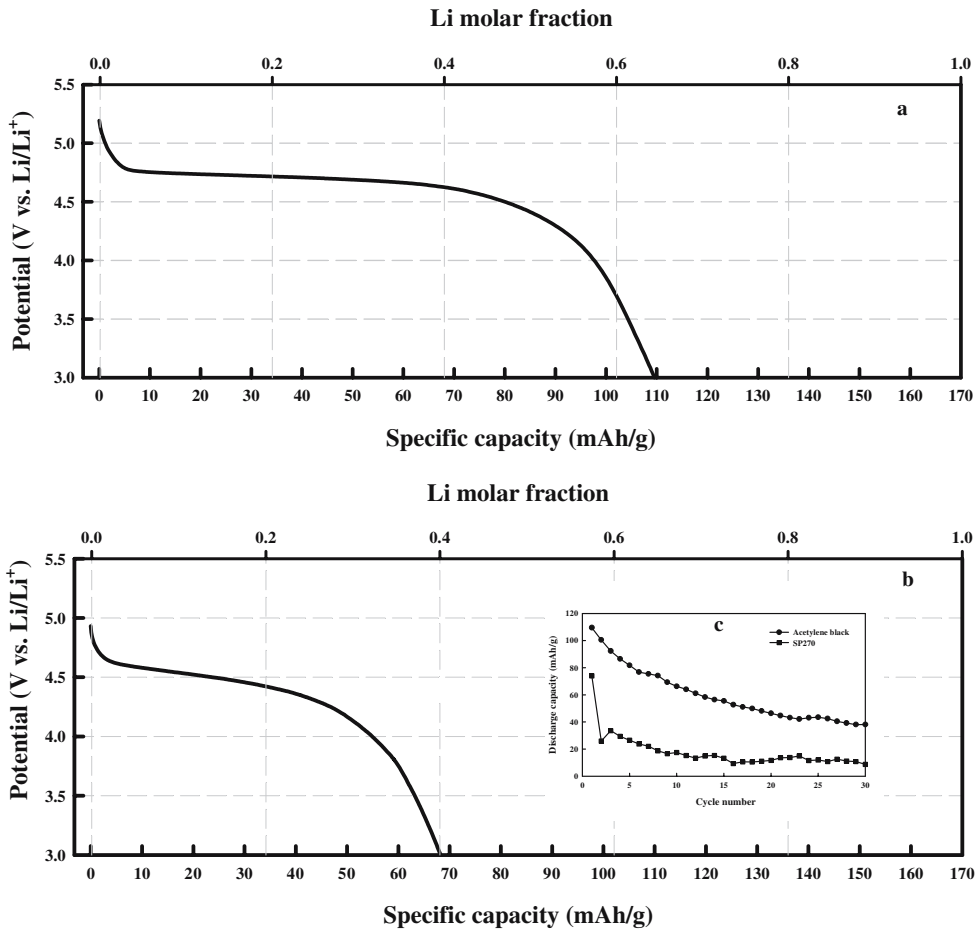

Fig. 6 The initial discharge curves of $LiCoPO_4$/Li batteries with different conductive additives (**a**) acetylene black and (**b**) carbon black (SP270) and (**c**) cycling performance of $LiCoPO_4$/Li batteries with different conductive additives

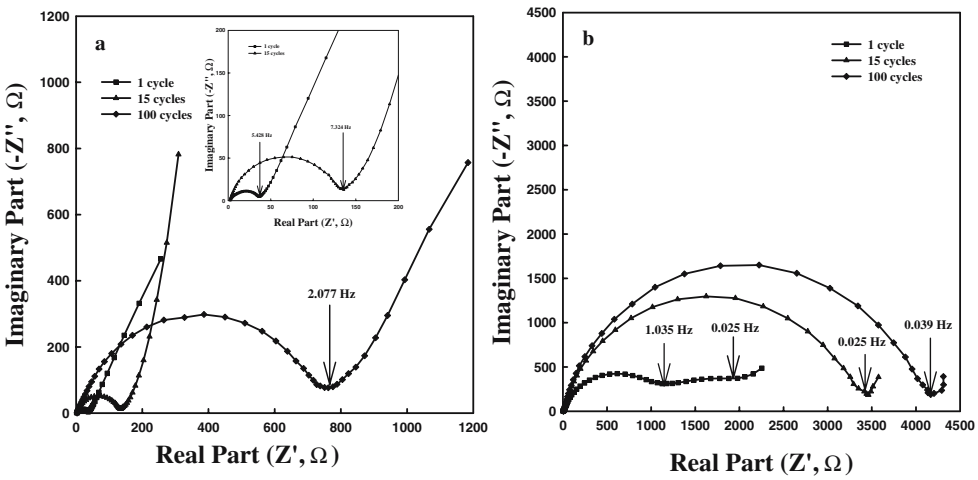

Fig. 7 Impedance spectra of $LiCoPO_4$/Li batteries with different conductive additives as a function of charge/discharge cycling (**a**) acetylene black and (**b**) carbon black (SP270)

tion. This is helpful to enhance the electrochemical properties of $LiCoPO_4$/Li batteries because of the increase in the quantity of $LiCoPO_4$ nanoparticles that can be used.

FE-SEM images of different conductive additives are shown in Fig. 3. As shown in Fig. 3a, the average particle size of spherical acetylene black is around 50 nm. As shown in Fig. 3b, the average particle size of plate-like carbon black (SP270) is around 250 nm, which is five times greater than spherical acetylene black nanoparticle.

FE-SEM images of the electrodes with different conductive additives are shown in Fig. 4. As can be seen in Fig. 4a, the distribution of $LiCoPO_4$ nanoparticles in acetylene black nanoparticles is generally homogeneous and the contact between $LiCoPO_4$ nanoparticles and acetylene black nanoparticles is fairly intimate. As shown in Fig. 4b, the distribution of $LiCoPO_4$ nanoparticles in SP270 is inhomogeneous and the contact between $LiCoPO_4$ nanoparticles and SP270 is poor.

Cyclic voltammograms of $LiCoPO_4$/Li batteries with different conductive additives are shown in Fig. 5. As for CV, the voltage difference between oxidation peak and reduction peak is an important parameter to value the electrochemical reaction reversibility [23]. As can be seen in Fig. 5a, during the first cycle, oxidation and reduction peaks appear at around 5.1 and 4.7 V, respectively. The voltage difference between two peaks is 0.4 V. As can be seen in Fig. 5b, during the first cycling, oxidation and reduction peaks appear at around 4.9 and 4.2 V, respectively. The voltage difference between two peaks is 0.7 V, which is greater than that of $LiCoPO_4$/Li battery with acetylene black. After seven cycles, in the case of acetylene back, the oxidation peak decreases and shifts to low potential. The corresponding reduction peak also decreases and hardly shifts to high or low potential; but in the case of SP270, the oxidation peak broadens and decreases and the corresponding reduction peak also decreases and hardly shifts to high or low potential. This is because of an increase in the internal impedance of battery upon charge/discharge cycling. As shown in Fig. 5a, the shoulder at about 4.8 V in the oxidation curve appears, indicating two-step mechanism of lithium deintercalation. The two-step mechanism of lithium deintercalation is under investigation. It is demonstrated that the reversibility and reactivity of $LiCoPO_4$/Li battery with acetylene black is better than that of $LiCoPO_4$/Li battery with SP270.

The initial discharge curves of $LiCoPO_4$/Li batteries with different conductive additives are presented in Fig. 6. The discharge plateaus appear at around 4.7 V (vs Li/Li^+) after initial charging, and this is consistent with the foregoing cyclic voltammetric data which show a reduction peak at around 4.7 V. The discharge curves seem to be characteristic for a one-step mechanism [12]. As shown in Fig. 6a, the initial discharge capacity of $LiCoPO_4$/Li battery with acetylene black is 110 mAh g^{-1}, the amount of cycled lithium is limited to 0.65. As shown in Fig. 6b, the initial discharge capacity of $LiCoPO_4$/Li battery with carbon black (SP270) is 68 mAh g^{-1}, the amount of cycled lithium is

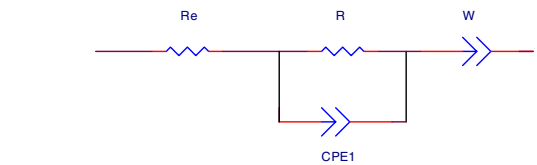

Model 1

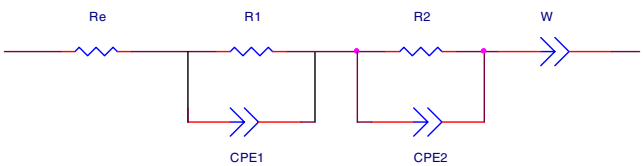

Model 2

Fig. 8 The simplified equivalent circuit models of $LiCoPO_4$/Li batteries to fit with the impedance spectra

Table 1 Impedance parameters calculated by equivalent circuit models of $LiCoPO_4$/Li batteries

Carbon sources	R_e[a](Ω)	R(Ω) 1st	R(Ω) 15th	R(Ω) 100th
Acetylene black	2.55	40	138	750
SP270	5.32	2,062	3,500	4,200

[a] Average value of R_e values in the 1st, 15th, and 100th cycles. $R=R_1+R_2$

limited to 0.4. As shown in Fig. 6c, the cycling performance of $LiCoPO_4$/Li batteries with different conductive additives is poor. In the meantime, it is obvious that the discharge property of $LiCoPO_4$/Li battery with acetylene black is better than that of $LiCoPO_4$/Li battery with carbon black (SP270), and it is consistent with the foregoing cyclic voltammetric data.

Impedance spectra of $LiCoPO_4$/Li batteries with different conductive additives as a function of charge-discharge cycling are shown in Fig. 7. It is noted that the ac impedance response of $LiCoPO_4$/Li battery forms a broad semicircle or two semicircles in high-to-medium frequency range and a line to the real axis in the lower frequency range. The semicircle in the high-to-medium frequency is mainly related to the complex reaction process at the electrolyte/cathode interface including resistance of SEI film formed on the surface $LiCoPO_4$ nanoparticles, the particle-to-particle contact resistance, charge transfer resistance, and corresponding capacitances. The inclined line in the lower frequency is attributed to the Warburg impedance, which is associated with lithium ion diffusion in $LiCoPO_4$ electrode.

The simplified equivalent circuit models are shown in Fig. 8 to evaluate the impedance spectra of $LiCoPO_4$/Li batteries after different cycles. Model 1 describes EIS with one semicircle and a linear part. Model 2 describes EIS with two semicircles and a linear part. The Li-ion migration resistance through the SEI film in the high frequency range is coded as R_1. The charge transfer resistance in the medium frequency range is coded as R_2. A sum of R_1 and R_2 is coded as R. An intercept at the Z_{real} axis in high frequency corresponds to the ohmic resistance (R_e), which represents the resistance of the electrolyte. The constant phase element (CPE) is a very general diffusion-related element and is commonly used for electrodes made from fine particles of active materials. W is the Warburg resistance. Table 1 shows the parameters of the equivalent circuit models of $LiCoPO_4$/Li batteries with different conductive additives after different cycles. As can be seen in Table 1, the resistance of $LiCoPO_4$/Li battery with acetylene black is 40 Ω at the first cycle, 138 Ω after 15 cycles, and 750 Ω after 100 cycles. The resistance of $LiCoPO_4$/Li battery with SP270 is 2062 Ω at the first cycle, 3500 Ω after 15 cycles, and 4200 Ω after 100 cycles. It is obvious that the resistance increases upon cycling. Two possible reasons for the increase in impedance: (1) crystalline structure of $LiCoPO_4$ cathode material might be destroyed upon charge/discharge cycling and (2) liquid electrolyte might be partially decomposed upon charge/discharge cycling. Detailed reasons are under investigation. It is noted that the resistance of $LiCoPO_4$/Li battery with acetylene black upon charge/discharge cycling is smaller than that of $LiCoPO_4$/Li battery with SP270. Therefore, as can be seen in Fig. 6, the discharge capacity of $LiCoPO_4$/Li battery with acetylene black is greater than that of $LiCoPO_4$/Li battery with SP270.

In the case of $LiCoPO_4$/Li battery with SP270, according to the equivalent circuit of model 2, there are two semicircles corresponding to SEI and charge transfer impedances after 1 cycle; the discharge capacity is 74 mAh g^{-1} after 1 cycle and 13 mAh g^{-1} after 15 cycles. It is obvious that there is a great decrease in capacity after 15 cycles; this is because of a great increase in resistance of battery from 2,062 to 3,500 Ω. The equivalent circuit of model 1 describes the impedance spectra of $LiCoPO_4$/Li battery with SP270 after 15 and 100 cycles; therefore, there is only one semicircle after 15 and 100 cycles.

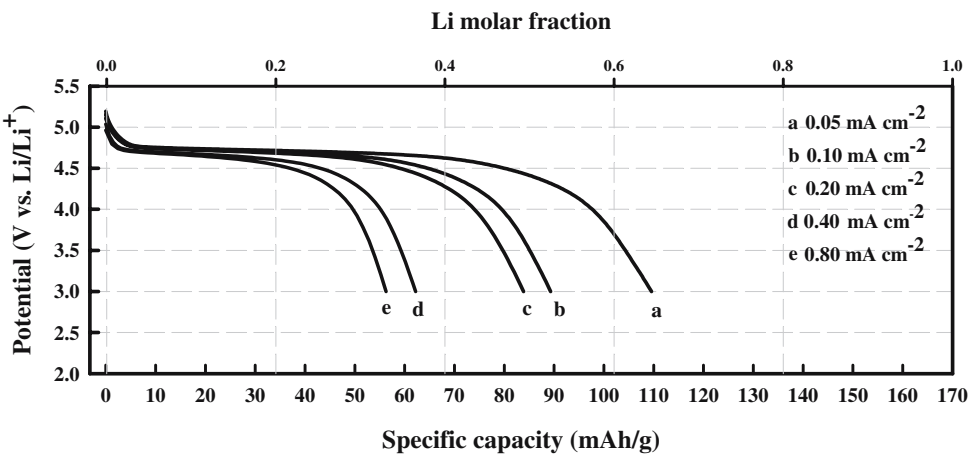

Fig. 9 The initial discharge curves of $LiCoPO_4$/Li battery with acetylene black at different current densities

The initial discharge curves of $LiCoPO_4$/Li battery with acetylene black at different current densities are shown in Fig. 9. The initial discharge capacity is 110 mAh g^{-1} at 0.05 mA cm^{-2}, 89 mAh g^{-1} at 0.10 mA cm^{-2}, 83 mAh g^{-1} at 0.20 mA cm^{-2}, 62 mAh g^{-1} at 0.40 mA cm^{-2}, and 56 mAh g^{-1} at 0.80 mA cm^{-2}. The potential plateau at around 4.7 V remains flat even for the 0.80 mA cm^{-2} curve. It indicates that the battery may operate at relatively high current densities, confirming the improved kinetics of $LiCoPO_4$ cathode materials. It is noted that the initial discharge capacity decreases as the current density increases. This phenomenon can be explained in terms of the electric polarization due to an increase in the *IR* drop, where *I* is the current passing the battery and *R* is the battery impedance. To improve the rate capability and charge/discharge cycling performance of $LiCoPO_4$, carbon coating will be carried out in the next step and the outcome will be reported in due course.

Conclusions

Single-phase $LiCoPO_4$ nanoparticles were synthesized by solid-state reaction method and subsequent high-energy ball milling. The XRD and TEM results showed that $LiCoPO_4$ nanoparticles had an orthorhombic olivine-type structure with a space group of Pmnb and average particle size of around 90–100 nm. Cyclic voltammograms, ac impedance experiments, and charge/discharge tests demonstrated that the electrochemical properties of $LiCoPO_4$/Li battery with acetylene black were the best. It exhibited a discharge plateau at around 4.7 V with an initial discharge capacity of 110 mAh g^{-1} at a discharge current density of 0.05 mA cm^{-2} at 25 °C. The charge/discharge tests at different current densities indicated that $LiCoPO_4$/Li battery with acetylene black could operate at relatively high current densities, confirming the improved kinetics of $LiCoPO_4$ cathode materials.

Acknowledgment The participants in this research received supporting funds from the second-stage BK 21.

References

1. Ozawa K (1994) Solid State Ionics 69:212
2. Pistoia G, Zane D, Zhang Y (1995) J Electrochem Soc 142:2551
3. Resimers JN, Dahn JR, von Sacken U (1993) J Electrochem Soc 140:2752
4. Li W, Resimers JN, Dahn JR (1993) Solid State Ionics 67:123
5. Dahn JR, von Sacken U, Juzkow MW, Al-Janaby H (1991) J Electrochem Soc 138:2207
6. Koetschau I, Richard MN, Dahn JR, Soupart JB, Rousche JC (1995) J Electrochem Soc 142:2906
7. Jeong I-S, Kim J-U, Gu H-B (2001) J Power Sources 102:55
8. Jin B, Kim J-U, Gu H-B (2003) J Power Sources 117:148
9. Kim J-U, Jo Y-J, Park G-C, Gu H-B (2003) J Power Sources 119–121:686
10. Jin B, Jun D-K, Gu H-B (2006) Trans Electr Electron Mater 7:76
11. Phadhi K, Nanjundaswamy KS, Goodenough JB (1997) J Electrochem Soc 144:1188
12. Bramnik NN, Bramnik KG, Buhrmester T, Baehtz C, Ehrenberg H, Fuess H (2004) J Solid State Electrochem 8:558
13. Amine K, Yasuda H, Yamachi M (2000) Electrochem Solid State Lett 3:178
14. Okada S, Sawa S, Egashira M, Yamaki J, Tabuchi M, Kageyama H, Konishi T, Yoshino A (2001) J Power Sources 97–98:430
15. Yamada A, Hosoya M, Chung S-C, Kudo Y, Hinokuma K, Liu K-Y, Nishi Y (2003) J Power Sources 119–121:232
16. Deniard P, Dulac AM, Rocquefelte X, Grigorova V, Lebacq O, Pasturel A, Jobic S (2004) J Phys Chem Solids 65:229
17. Loris JM, Perez-Vicente C, Tirado JL (2002) Electrochem Solid State Lett 5:A234
18. Li G, Azuma H, Tohda M (2002) Electrochem Solid State Lett 5: A135
19. Jeon Y-S, Jin EM, Jin B, Jun D-K, Han ZJ, Gu H-B (2007) Trans Electr Electron Mater 8:41
20. Kwon SJ, Kim CW, Jeong WT, Lee KS (2004) J Power Sources 137:93
21. Jeong WT, Lee KS (2002) J Power Sources 104:95
22. Rabanal ME, Gutierrez MC, Garcia-Alvarado F, Gonzalo EC, Arroyo-de Dompablo ME (2006) J Power Sources 160:523
23. Ni JF, Zhou HH, Chen JT, Zhang XX (2005) Mater Lett 59:2361